Equations of state and stability of color-superconducting quark matter cores in hybrid stars

B. K. Agrawal*

Saha Institute of Nuclear Physics, Kolkata-700064, India

(Received 6 November 2009; published 28 January 2010)

The stable configurations of nonrotating and rotating hybrid stars composed of color-superconducting quark matter cores are constructed using several equations of state (EOSs). We use a set of diverse EOSs for the nuclear matter which represents the low density phase. The EOSs at higher densities correspond to the quark matter in the color-superconducting phase and are computed within the Nambu-Jona-Lasinio-like model for different values of the scalar diquark and vector current couplings strengths. The phase transition to the quark matter is computed by a Maxwell construction. We find that the stability of the hybrid stars are mainly governed by the behavior of the EOSs for the color-superconducting quark matter. However the compositions of hybrid stars are sensitive to the EOS of the nuclear matter. The value of the critical rotation frequency for the hybrid star depends strongly on the EOS of the nuclear matter as well as that for the color-superconducting quark matter. Our results indicate that the EOS for the color-superconducting quark matter can be obtained, by adjusting the parameters of the Nambu-Jona-Lasinio model, to yield the stable configurations of the hybrid star having the maximum mass $\sim 1.5 M_{\odot}$ in the nonrotating limit and the critical rotation frequency ~ 1 kHz.

DOI: 10.1103/PhysRevD.81.023009 PACS numbers: 97.60.Jd, 12.38.−t, 26.60.Kp

I. INTRODUCTION

The present knowledge of quantum chromodynamics (QCD) suggests that quark matter might be in different color-superconducting phases at high densities. Thus, one expects the core of the hybrid stars to be composed of color-superconducting quark matter (CSQM) surrounded by a nuclear mantle. The possible CSQM phases are the two-flavor color superconductor (2SC) [1–3], the color flavour locked (CFL) phase [4,5], and crystalline color superconductor [6,7]. The speculation that the CSQM exists in the core of the hybrid stars has triggered many theoretical investigations both on the modeling of the equation of state (EOS) of quark matter and on the phenomenological signatures of the presence of quark matter in the compact stars [8].

The nuclear matter phase of the hybrid star is described by the various models which can be broadly grouped into (i) nonrelativistic potential models [9], (ii) nonrelativistic mean-field models [10–13], (iii) field theoretical based relativistic mean-field models [14–16], and (iv) Dirac-Brueckner-Hartree-Fock models [17–20]. The quark matter in the color-superconducting phases are usually described either within the Massachusetts Institute of Technology (MIT) bag model or using a more realistic Nambu-Jona-Lasinio (NJL) like model. The studies based on the MIT bag model indicate the existence of stable configurations of hybrid stars with the CFL quark matter core [21–24]. Further, the MIT bag model predicts the absence of the 2SC color-superconducting phase in the hybrid stars [25]. The scenario is somewhat different when the NJL model is employed to study the hybrid stars with CSQM core. The stable configurations of hybrid stars with 2SC quark matter core are possible within the NJL model [26–29]. However, earlier investigations [30–32] based on the NJL model ruled out the possibility of CFL quark matter at the core of the hybrid stars, because it rendered the hybrid star unstable. Only very recently [33,34], it has been demonstrated that inclusion of the six-fermion interaction term together with large enough values of the scalar diquark coupling strength in the NJL model can yield stable configurations of the hybrid star containing 2SC or CFL quark matter core. The NJL model is also applied to study the possibility of existence of the crystalline color superconductor quark matter phase in the hybrid stars [35,36].

The stability and the structure of the nonrotating hybrid stars are quite sensitive to the choice of the EOS of the nuclear matter and the quark matter [21,37]. Further, one often finds that even though the stable configurations of the nonrotating hybrid star for a given EOS belong to the third family of compact stars, but, the maximum rotation frequency up to which these hybrid stars are stable is much lower than the corresponding mass-shedding (Keplerian) frequency [38,39]. The EOSs for the quark matter in the unpaired or in the various color-superconducting phases employed in these investigations were obtained within the MIT bag model. Recently [40], a more realistic EOS for the unpaired quark matter computed within the NJL model is used to show that the maximum mass of the nonrotating hybrid stars depends sensitively on the choice of the EOS of the nuclear matter. It is necessary to construct stable configurations of the nonrotating and rotating hybrid stars using realistic EOSs for the nuclear matter and for the quark matter in the color-superconducting phases.

In the present work, we compute several EOSs and use them to study the properties of the nonrotating and rotating hybrid stars composed of CSQM core. The lower density

*bijay.agrawal@saha.ac.in

part of these EOSs correspond to the nuclear matter and are based on the variational and mean-field approaches. Our set of EOSs for the nuclear matter around the saturation density ($\rho_0 = 0.16$ fm^{-3}) is constrained by the bulk properties of the finite nuclei. But, their behavior at densities, $\rho > \rho_0$, are significantly different. The EOSs for CSQM are calculated within the NJL model using different values for the scalar diquark and vector current coupling strengths. The EOS at intermediate densities are obtained using a Maxwell construction.

The paper is organized as follows: in Sec. II we describe, in brief, the models employed to construct the EOSs for nuclear matter and the CSQM. In Sec. III we present the results for the equilibrium sequences for nonrotating and rotating hybrid stars. In Sec. IV we state our conclusions.

II. EQUATIONS OF STATE

We compute the EOSs which correspond to the nuclear matter at lower densities and CSQM in the 2SC or CFL phases at higher densities. The EOS at intermediate densities are obtained using a Maxwell construction. For nuclear matter in the β equilibrium, we employ a set of diverse EOSs which are obtained using various approaches, like variational, nonrelativistic mean field (NRMF) and relativistic mean field (RMF). In Fig. 1 we plot various nuclear matter EOSs. The low density behavior of these EOSs are very much similar as they are constrained by the bulk properties of the finite nuclei. But, their behavior at higher densities are so different that the resulting neutron star properties are at variance. In Table I, we list some key properties of the nonrotating neutron stars obtained using these nuclear matter EOSs. It can be seen from Table I that the values of the maximum neutron star masses are in the range of 2.0–2.8$M_\odot$ and the radius $R_{1.4}$ at the canonical neutron star mass vary between 11.3–14.8 km. It is interesting to note that the values of the maximum neutron star mass for both the APR and TM1 EOSs are equal, but the radius at the canonical mass of the neutron star is reasonably smaller for the APR EOS. This is due to the fact that the APR EOS is softer relative to the TM1 at intermediate densities and it becomes stiffer at high densities as can be seen from Fig. 1. Similar is the case with SLY4 and BSR10 EOSs. We shall see in the next section that these pairs of nuclear matter EOSs, for which the maximum neutron star masses are the same, yield significantly different structure for the hybrid stars.

The EOSs for the CSQM in the 2SC or CFL phase are obtained within the NJL model. The input variables of the NJL model are the chemical potentials for all the quark flavours and colors in the chemical equilibrium which is given by the matrix

$$\mu_{ab}^{\alpha\beta} = (\mu\delta^{\alpha\beta} + \mu_Q Q_f^{\alpha\beta})\delta_{ab} + [\mu_3(T_3)_{ab} + \mu_8(T_8)_{ab}]\delta^{\alpha\beta}, \quad (1)$$

where, μ is the quark chemical potential, μ_Q is the chemical potential of the electric charge equal to minus the electron chemical potential μ_e, and μ_3 and μ_8 are the color chemical potentials associated with the two mutually commuting color charges of the $SU(3)_c$ gauge group. The explicit form of the electric charge matrix $Q_f = \mathrm{diag}_f(\frac{2}{3}, -\frac{1}{3}, -\frac{1}{3})$, and for the color charge matrices $T_3 = \mathrm{diag}_c(\frac{1}{2}, -\frac{1}{2}, 0)$, and $\sqrt{3}T_8 = \mathrm{diag}_c(\frac{1}{2}, \frac{1}{2}, -1)$. In the mean-field approximation, the pressure at vanishing temperature reads as,

$$p = 4K\sigma_u\sigma_d\sigma_s - \frac{1}{4G_D}\sum_{c=1}^{3}|\Delta_c|^2 - 2G_S\sum_{\alpha=1}^{3}\sigma_\alpha^2 + \frac{\omega_0^2}{4G_V} + \frac{1}{2\pi^2}\sum_{i=1}^{18}\int_0^\Lambda dk k^2|\epsilon_i| + P_e - B \quad (2)$$

where, $\sigma_{u,d,s}$ are the quark-antiquark condensates and Δ_c are the three diquark condensates. The values of σ_i and Δ_c are determined using

$$\frac{\partial p}{\partial \sigma_i} = 0 \quad (3)$$

TABLE I. Values of the maximum mass $M_{\max}$ and corresponding central energy density $\epsilon_{\max}$ and radius $R_{\max}$ obtained for different EOSs of the nuclear matter. The radius $R_{1.4}$ for the neutron star with canonical mass (1.4 $M_\odot$) are also given.

EOS	Approach	$\epsilon_{\max}$ (10^{15} g/cm^3)	$M_{\max}$ ($M_\odot$)	$R_{\max}$ (km)	$R_{1.4}$ (km)	Ref.
APR	Variational	2.80	2.19	9.9	11.3	[41]
SLY4	NRMF	2.84	2.05	10.0	11.7	[42]
BSR10 [a]	RMF	2.14	1.97	11.6	13.3	[43]
TM1	RMF	1.87	2.19	12.4	14.4	[44]
NL3	RMF	1.55	2.79	13.3	14.7	[45]

[a]This EOS is obtained using one of the several parameter sets of the extended RMF model given in our earlier work [43]. Each of these parametrizations corresponds to different values of the strength ζ for the ω meson self-coupling term and neutron-skin thickness Δr in ^{208}Pb nucleus. The remaining parameters of the models were calibrated to yield reasonable fit to the bulk nuclear observables and nuclear matter incompressibility coefficient. In the present work we use the parameter set with $\zeta = 0.03$ and $\Delta r = 0.2$ fm which will be referred henceforth as BSR10.

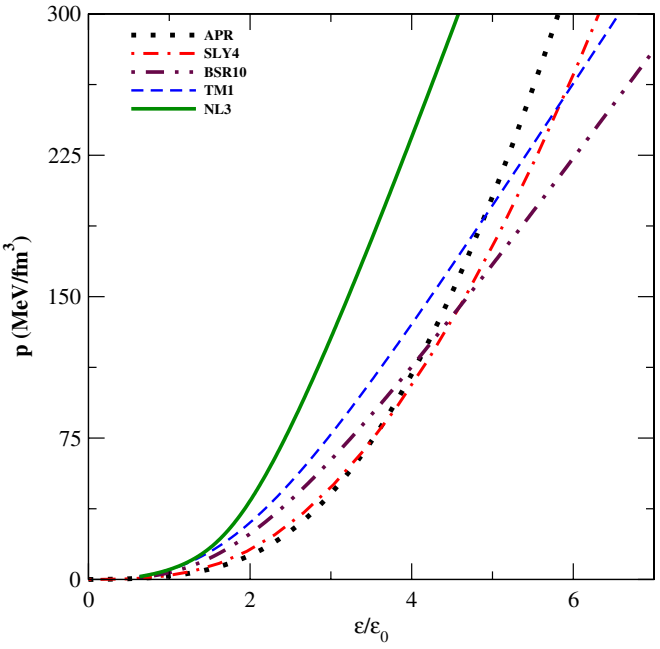

FIG. 1 (color online). The nuclear matter EOSs plotted as pressure versus energy density. The energy density is normalized by $\epsilon_0 = 150$ MeV/fm^3 which is the typical value of the energy density for the nuclear matter at the saturation density.

$$\frac{\partial p}{\partial \Delta_c} = 0. \tag{4}$$

In Eq. (2) ω_0 is the mean-field expectation value for isoscalar vector like meson ω given as [32] $\omega_0 = 2G_V\langle QM \mid \psi_u^\dagger \psi_u + \psi_d^\dagger \psi_d + \psi_s^\dagger \psi_s \mid QM\rangle$. This field modifies also the chemical potentials: $\mu_{u,d,s} \rightarrow \mu_{u,d,s} - \omega_0$. The ϵ_i are the dispersion relations computed by following Ref. [3]. The ϵ_i depend explicitly on the values of current quark masses, quark-antiquark and diquark condensates, and various chemical potentials appearing in Eq. (1). The $P_e = \mu_e^4/(12\pi^2)$ is the contribution to the pressure from the electrons. The constant B is so determined that the pressure vanishes at zero density and temperature. In addition to the Eqs. (3) and (4), the pressure must satisfy,

$$n_Q \equiv \frac{\partial p}{\partial \mu_Q} = 0, \tag{5}$$

$$n_3 \equiv \frac{\partial p}{\partial \mu_3} = 0, \tag{6}$$

$$n_8 \equiv \frac{\partial p}{\partial \mu_8} = 0, \tag{7}$$

so that local electric and color charge neutrality conditions are met. Once the pressure as a function of quark chemical potential is known, quark matter EOS can be easily computed.

The model parameters, the current quark masses $m_{u,d,s}$, quark-antiquark coupling G_S, the strength K of the six-fermion or "'t Hooft" interaction and the cutoff parameter Λ are taken to be [46],

$$m_u = m_d = 5.5 \text{ MeV}, \tag{8}$$

$$m_s = 140.7 \text{ MeV}, \tag{9}$$

$$G_S\Lambda^2 = 1.835, \tag{10}$$

$$K\Lambda^5 = 12.36, \tag{11}$$

$$\Lambda = 602.3 \text{ MeV}. \tag{12}$$

After fixing the masses of the up and down quarks, $m_u = m_d = 5.5$ MeV, the other four parameters are chosen to reproduce the following observables of vacuum QCD [46]: $m_\pi = 135.0$ MeV, $m_K = 497.7$ MeV, $m_{\eta'} = 957.8$ MeV, and $f_\pi = 92.4$ MeV. This parameter set gives $m_\eta = 514.8$ MeV. The value of B for this set of parameters is $(425.4 \text{ MeV})^4$. There are two more parameters, the diquark coupling strength G_D and the vector current coupling strength G_V, which are not known. One expects that the diquark coupling has a similar strength as the quark-antiquark coupling. We construct quark matter EOS for $G_D = 1.1$–$1.2G_S$ with $G_V = 0$–$0.2G_S$.

In the 2SC phase, pairing occurs only between the u and d quarks and the s quarks remain unpaired leading to $\Delta_1 = \Delta_2 = 0$ and $\Delta_3 \neq 0$. On the other hand, in the CFL phase, $\Delta_1 \neq 0$, $\Delta_2 \neq 0$, and $\Delta_3 \neq 0$. In the left panels of Figs. 2 and 3, we plot the pressure as a function of the quark chemical potential for the nuclear matter and for the quark matter in the 2SC and CFL phases. The phase realized at a given chemical potential is the one having largest pressure. Thus, it is evident from the $P - \mu$ curves that direct transition from nuclear matter to the CFL quark matter occurs for the case of APR and SLY4 EOSs. For the TM1 and NL3 EOSs, transition from nuclear matter to the CFL quark matter proceeds via 2SC phase at intermediate densities. For the BSR10 EOS, nuclear matter to CFL quark matter phase transition proceeds via 2SC phase only for $G_D = 1.2\ G_S$ with $G_V = 0$. We see from these figures that the pressure, at which the transition from the nuclear to quark matter occurs, decreases with increasing G_D or decreasing G_V. For instance, pressure at the phase transition reduces almost by a factor of 2 with increase in G_D from 1.1 G_S to 1.2 G_S. The solid circles on the various EOSs for the nuclear matter indicate the values of $P_{1.4}$ which is the pressure at the center of the neutron star with the canonical mass (1.4 $M_\odot$). The values of transition pressure is close to that of $P_{1.4}$ for the cases plotted in the lower and the upper panels of Figs. 2 and 3, respectively. For the completeness, in the right panels of Figs. 2 and 3, we display the plots for the pressure as a function of the baryon density for the case of APR, BSR10, and NL3

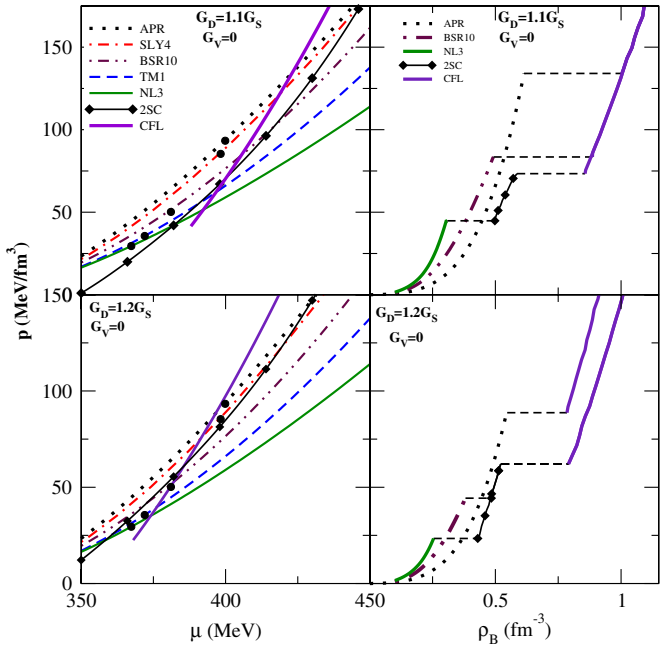

FIG. 2 (color online). The pressure as a function of the quark chemical potential (left panel) and the baryon density (right panel) for the nuclear and quark matter. The EOSs for the quark matter in the 2SC and CFL phases are obtained within the NJL model using $G_V = 0$ with $G_D = 1.1G_S$ and $1.2G_S$. The solid circles on the various EOSs for the nuclear matter indicate the pressure at the center of the neutron star with the canonical mass ($1.4\ M_\odot$).

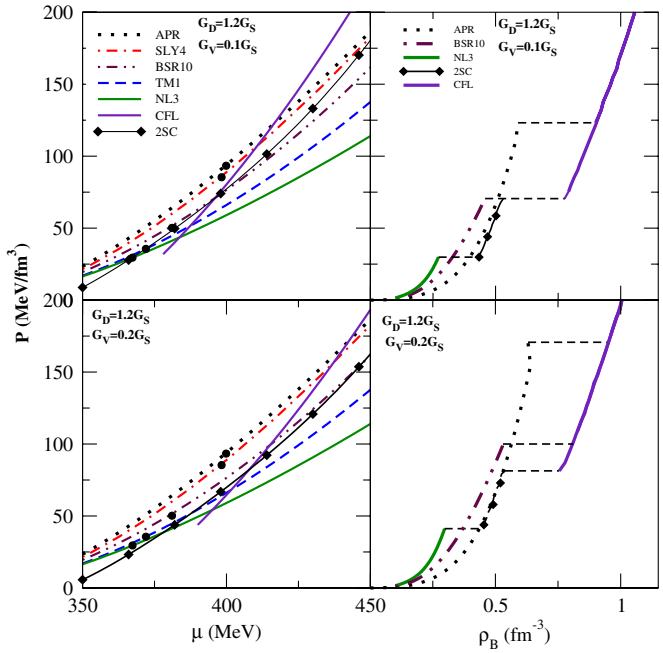

FIG. 3 (color online). Same as Fig. 2, but, for $G_V = 0.1\ G_S$ and $0.2\ G_S$ with $G_D = 1.2\ G_S$.

EOSs. The phase transition to the quark matter is computed by a Maxwell construction.

III. HYBRID STARS WITH CSQM CORE

We construct the equilibrium sequences of the nonrotating and rotating compact stars using the EOSs obtained in the last section. These EOSs correspond to the nuclear matter at lower densities and the CSQM in the 2SC or CFL phase at higher densities as shown in Figs. 2 and 3. The nuclear matter EOSs are taken from the published literature as summarized in Table I. The EOSs for the CSQM are computed within the NJL model for different values of the scalar diquark coupling strength G_D and the vector current coupling strength G_V. The other parameters of the model are determined by fit to some of the observables of the vacuum QCD. The various EOSs as obtained in the present work can be completely specified by (i) the source for the nuclear matter EOS as listed in Table I and (ii) the values of G_D and G_V used in computing the EOS of the CSQM within the NJL model. The properties of spherically symmetric nonrotating and axially symmetric rotating compact stars are obtained by solving the Einstein's equations in one dimension and two dimensions, respectively. The numerical computations are performed by using computer code written by Stergioulas and Friedman [47].

The equilibrium sequence of compact stars for a given EOS is obtained by varying the central energy density ϵ_c. For the stable configuration,

$$\frac{\partial M}{\partial \epsilon_c} \geq 0, \tag{13}$$

where, M is the gravitational mass of the nonrotating compact star. The equilibrium sequences for the nonrotating compact stars resulting from our EOSs are plotted as mass versus radius in Figs. 4 and 5. The central energy density increases as we move along these curves from the right hand side. The portion of the curves left to the solid circles represent the equilibrium sequences of hybrid stars with CFL quark matter core. The curves between the solid circle and triangle represent the sequences of hybrid star composed of 2SC quark matter core. It is clear from the lower panel of Fig. 4 and upper panel of Fig. 5 that the stable configurations of hybrid stars with CFL quark matter core belong to third family of compact stars. Further, irrespective of the choice of the EOS of the nuclear matter, the stable configurations of the nonrotating hybrid stars exist within the NJL model only when the EOSs for the CSQM are constructed for $G_D = 1.2\ G_S$ with $G_V \lesssim 0.1\ G_S$. These values of G_D and G_V, for which the stable configurations of the hybrid star exist, are very much similar to the ones found in Ref. [33]. It appears that the stability of the hybrid stars with CSQM core depends solely on the choice of the EOS for the CSQM. However, the composition of the hybrid stars depend on the behavior of the nuclear matter EOS. For instance, in case of the TM1

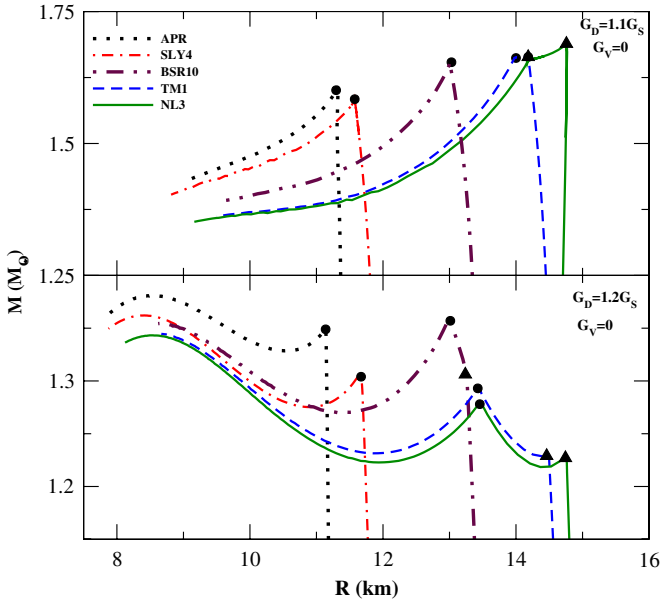

FIG. 4 (color online). Plots for the mass-radius relationships for the equilibrium sequences of nonrotating compact stars obtained using various EOSs as shown in Fig. 2. The curves on the left of the solid circles represent the equilibrium sequences for the hybrid stars with core composed of the quark matter in the CFL phase. The curves between the solid circles and triangles represent the hybrid stars with 2SC quark matter core. The absence of solid triangle on a curve means that the hybrid stars contain quark matter only in the CFL phase.

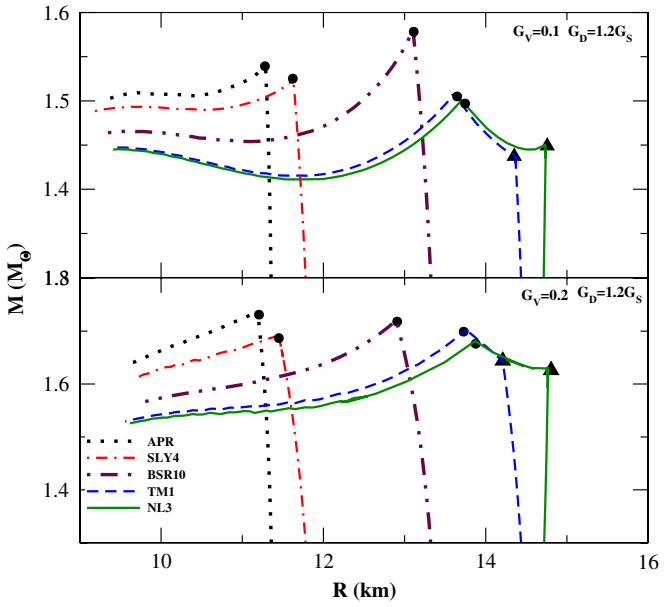

FIG. 5 (color online). Plots for the mass-radius relationships for the equilibrium sequences of the nonrotating compact stars obtained using various EOSs as shown in Fig. 3. The solid circles and triangles divide the curves according to the composition of the hybrid stars as described in Fig. 4.

and the NL3 EOSs of the nuclear matter, the core of the hybrid stars are composed of CSQM which is either in 2SC phase or in the CFL phase. In the later case, CFL quark matter core is surrounded by a layer of 2SC quark matter with the outer layer composed of nuclear matter. The thickness of the 2SC quark matter at the maximum hybrid star mass is around 0.5–0.7 km and its mass is $\sim 0.1\ M_\odot$. On the other hand, no 2SC quark matter appears in the stable configurations of the hybrid star constructed using the EOSs for which the nuclear matter part correspond to the APR and SLY4.

The equilibrium sequences for the hybrid stars rotating with fixed rotation frequency f are constructed. As an illustration, in Fig. 6, we plot mass versus circumferential equatorial radius $R_{\rm eq}$ at fixed values of the rotational frequency obtained for two different EOSs. For the clarity, we mainly focus on the regions of the $M - R_{\rm eq}$ curves corresponding to the sequences of the hybrid stars which are relevant in the present context. We see that beyond certain frequency, so-called the critical rotation frequency $f_{\rm crit}$, the stable configuration for the rotating hybrid star does not exist. The solid black lines in Fig. 6 represent the result obtained at the $f = f_{\rm crit}$. In Fig. 7 we plot the values for the $f_{\rm crit}$ (left panel) calculated for the cases for which the stable configurations for the nonrotating hybrid star exist. It is evident that the values of $f_{\rm crit}$ are quite sensitive to the choice of the EOS for the nuclear matter as well as the CSQM. Depending on the EOSs, $f_{\rm crit}$ varies in the range of 350–1275 Hz. We also plot in Fig. 7 (right panel) the maximum mass $M_{\rm max}$ for the nonrotating hybrid stars

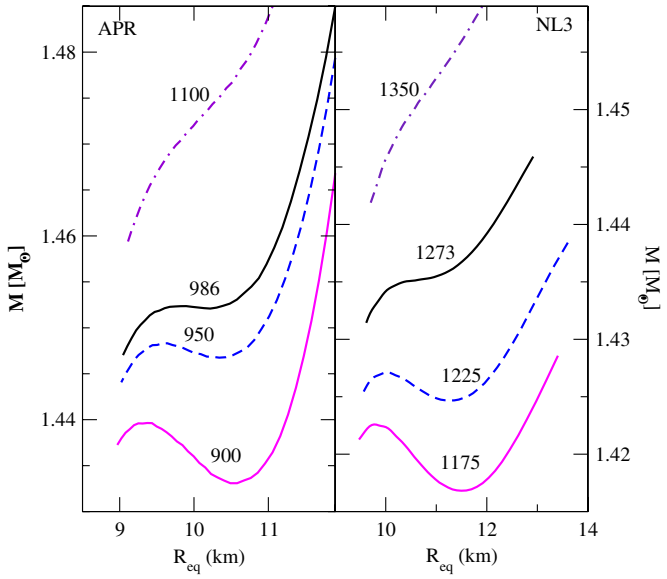

FIG. 6 (color online). Plots for the mass versus circumferential equatorial radius $R_{\rm eq}$ at fixed values of the rotational frequency as indicated along each of the curves (in Hz). The black solid lines represent the results obtained at the critical frequencies $f_{\rm crit}$. For $f > f_{\rm crit}$, the stable configurations of hybrid star do not exist.

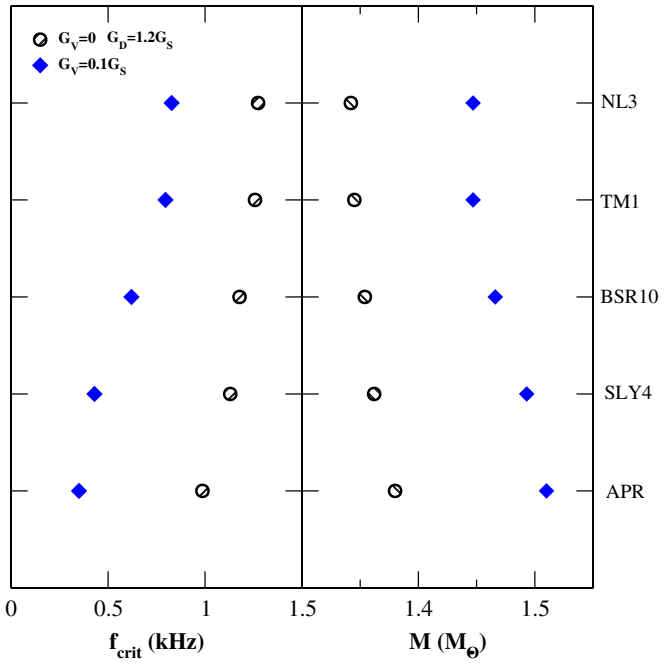

FIG. 7 (color online). The values of the critical rotation frequency $f_{\rm crit}$ (left panel) for the hybrid stars with the CSQM core and their maximum masses (right panel) in the nonrotating limit as obtained using different EOSs for the nuclear matter and the CSQM.

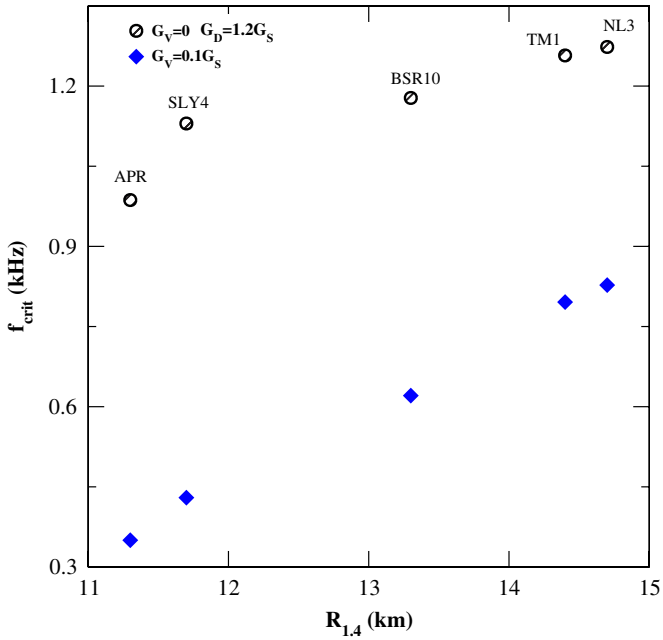

FIG. 8 (color online). Correlations between values of $f_{\rm crit}$ for the hybrid stars and the radius $R_{1.4}$ for the neutron star with canonical mass as listed in Table I.

with CSQM core. It is interesting to note from this figure that the values of G_D and G_V for a given nuclear matter EOS can be so adjusted that the resulting hybrid star has (a) the maximum mass in the nonrotating limit larger than 1.44 $M_\odot$ which is the most accurately measured value for the maximum mass of a compact star [48] and (b) the maximum allowed rotation frequency is larger than the current observational limit of 716 Hz [49].

In Fig. 8 we show the correlations between the values of the $f_{\rm crit}$ for the hybrid stars and the radius $R_{1.4}$ for the neutron star with the canonical mass. We see that $f_{\rm crit}$ is large if the value of $R_{1.4}$ is also large. Thus, the hybrid star constructed for a given EOS for the CSQM can rotate faster if the EOS for the nuclear matter is stiffer. The existence of the correlations between the values of $f_{\rm crit}$ and $R_{1.4}$ may be due to the fact that the pressure at which the nuclear to the quark matter transition occurs is closer to the values of $P_{1.4}$ as can be seen from the lower and upper left panels of Figs. 2 and 3, respectively.

Finally, we would like to compare the present results with corresponding ones obtained within the MIT bag model [37,50]. The present results as obtained within the NJL model are significantly different with those for the MIT bag model. Within MIT bag model the EOS for the CSQM can be obtained by adjusting the value of the CFL gap parameter and the bag constant such that the resulting hybrid stars with CFL quark matter core are gravitationally stable up to the masses ~ 2 $M_\odot$ in the static limit and the maximum allowed rotation frequency is much larger than 1 kHz. However, it can be seen from Fig. 7, stable configurations of the hybrid stars with CFL quark matter core obtained within the NJL model are having the maximum values for the mass and the rotational frequency appreciably lower than those obtained for the MIT bag model. The differences between the results for the MIT bag model and the NJL model can be attributed to the fact that the constituent quark masses, chiral condensates and the color-superconducting gaps in the later case are computed self-consistently as a function of baryon density.

IV. CONCLUSIONS

The stability of nonrotating and rotating hybrid stars, composed of the color superconducting quark matter core surrounded by a nuclear mantle, is studied by using several EOSs. The EOSs for the nuclear matter, employed at lower densities, are based on the variational and the mean-field approaches. We use a diverse set of nuclear matter EOSs such that the resulting maximum neutron star mass lies in the range of 2.2–2.8 $M_\odot$ and the radius at the canonical neutron star mass vary between 11.3–14.8 km. The EOSs at higher densities corresponding to the color-superconducting quark matter in the 2SC or the CFL phase, are calculated within the NJL model using different values of coupling strengths for the scalar diquark and isoscaler vector terms. The EOS at intermediate densities are obtained using a Maxwell construction.

We find that the stability of the nonrotating hybrid stars is very much sensitive to the EOSs for the color-

superconducting quark matter and almost independent of the choice for the EOS for the nuclear matter. The stable configurations of the hybrid stars exist only for the large enough value for the scalar diquark coupling strength. Though, the stability of the hybrid stars are not sensitive to the choice of the EOSs for the nuclear matter, but compositions of the hybrid stars are at variance for these EOSs. If the EOS for the nuclear matter is stiff, core of the hybrid star is composed of color-superconducting quark matter which is either in the 2SC or the CFL phase. In the later case, CFL quark matter core is surrounded by a thin layer of the 2SC quark matter and the outer layer composed of nuclear matter.

The stability of the rotating hybrid star is sensitive to the choice of the EOS for the nuclear matter as well as that for the color-superconducting quark matter. In particular, we find that the values of the critical rotation frequency vary from about 350 Hz to 1275 Hz depending upon the choice of the EOSs for the nuclear matter and the color-superconducting quark matter. Our results also indicate that the EOSs for the color-superconducting quark matter obtained within the NJL model may be adjusted for the various nuclear matter EOSs in such a way that it yields (a) the maximum mass in the nonrotating limit larger than 1.44 $M_\odot$ which is the most accurately measured value for the maximum mass of a compact star and (b) the maximum allowed rotation frequency is larger than the current observational limit of 716 Hz.

Finally, we would like to mention that our present study can be extended in several ways. The quark matter in the crystalline color-superconducting phase, expected to appear at the intermediate densities, should also be considered. One might also include the contributions from the hyperons which would soften the hadronic EOS. The phase transition from hadron to the quark matter should proceed via mixed phase which can be constructed using the Gibbs conditions.

[1] M. G. Alford, K. Rajagopal, and F. Wilczek, Phys. Lett. B **422**, 247 (1998).
[2] S. B. Rüster and D. H. Rischke, Phys. Rev. D **69**, 045011 (2004).
[3] S. B. Rüster, V. Werth, M. Buballa, I. A. Shovkovy, and D. H. Rischke, Phys. Rev. D **72**, 034004 (2005).
[4] M. G. Alford, K. Rajagopal, and F. Wilczek, Nucl. Phys. **A537**, 443 (1999).
[5] K. Rajagopal and F. Wilczek, Phys. Rev. Lett. **86**, 3492 (2001).
[6] M. G. Alford, J. Bowers, and K. Rajagopal, Phys. Rev. D **63**, 074016 (2001).
[7] K. Rajagopal and R. Sharma, Phys. Rev. D **74**, 094019 (2006).
[8] M. G. Alford, A. Schmitt, and T. Schfer, Rev. Mod. Phys. **80**, 1455 (2008).
[9] V. R. Pandharipande and R. A. Smith, Nucl. Phys. **A237**, 507 (1975).
[10] E. Chabanat, P. Bonche, P. Haensel, J. Meyer, and R. Schaeffer, Nucl. Phys. **A627**, 710 (1997).
[11] J. R. Stone, J. C. Miller, R. Koncewicz, P. D. Stevenson, and M. R. Strayer, Phys. Rev. C **68**, 034324 (2003).
[12] L. Mornas, Eur. Phys. J. A **24**, 293 (2005).
[13] B. K. Agrawal, S. K. Dhiman, and R. Kumar, Phys. Rev. C **73**, 034319 (2006).
[14] M. Prakash, J. R. Cooke, and J. M. Lattimer, Phys. Rev. D **52**, 661 (1995).
[15] N. K. Glendenning and J. Schaffner-Bielich, Phys. Rev. C **60**, 025803 (1999).
[16] A. W. Steiner, M. Prakash, J. M. Lattimer, and P. Ellis, Phys. Rep. **411**, 325 (2005).
[17] H. Müther, M. Prakash, and T. L. Ainsworth, Phys. Lett. B **199**, 469 (1987).
[18] L. Engvik, M. Hjorth-Jensen, E. Osnes, G. Bao, and E. Østgaard, Phys. Rev. Lett. **73**, 2650 (1994).
[19] L. Engvik, E. Osnes, M. Hjorth-Jensen, G. Bao, and E. Østgaard, Astrophys. J. **469**, 794 (1996).
[20] H. J. Schulze, A. Polls, A. Ramos, and I. Vidana, Phys. Rev. C **73**, 058801 (2006).
[21] M. Alford and S. Reddy, Phys. Rev. D **67**, 074024 (2003).
[22] S. Banik and D. Bandyopadhyay, Phys. Rev. D **67**, 123003 (2003).
[23] A. Drago, A. Lavagno, and G. Pagliara, Phys. Rev. D **69**, 057505 (2004).
[24] I. Bombaci, G. Lugones, and I. Vidana, Astron. Astrophys. **462**, 1017 (2007).
[25] M. Alford and K. Rajagopal, J. High Energy Phys. 06 (2002) 031.
[26] D. Blaschkel, S. Fredriksson, H. Grigorian, A. M. zta, and F. Sandin, Phys. Rev. D **72**, 065020 (2005).
[27] D. N. Aguilera, D. Blaschke, and H. Grigorian, Astron. Astrophys. **416**, 991 (2004).
[28] D. N. Aguilera, D. Blaschke, and H. Grigorian, Nucl. Phys. **A757**, 527 (2005).
[29] H. Grigorian, D. Blaschke, and D. N. Aguilera, Phys. Rev. C **69**, 065802 (2004).
[30] M. Baldo, M. Buballa, F. Burgio, F. Neumann, M. Oertel, and H. Schulze, Phys. Lett. B **562**, 153 (2003).
[31] M. Buballa, Phys. Rep. **407**, 205 (2005).
[32] T. Klähn, D. Blaschke, F. Sandin, C. Fuchs, A. Faessler, H. Grigorian, G. Ropke, and J. Trümper, Phys. Lett. B **654**, 170 (2007).
[33] G. Pagliara and J. Schaffner-Bielich, Phys. Rev. D **77**, 063004 (2008).
[34] A. Drago, G. Pagliara, and J. Schaffner-Bielich, J. Phys. G **35**, 014052 (2008).

[35] N. D. Ippolito, M. Nardulli, and M. Ruggieri, J. High Energy Phys. 04 (2007) 036.
[36] N. D. Ippolito, M. Ruggieri, D. H. Rischke, A. Sedrakian, and F. Weber, Phys. Rev. D **77**, 023004 (2008).
[37] M. Alford, M. Braby, M. Paris, and S. Reddy, Astrophys. J. **629**, 969 (2005).
[38] S. Banik, M. Hanauske, and D. Bandyopadhyay, J. Phys. G **31**, S841 (2005).
[39] A. Bhattacharyya, S. K. Ghosh, M. Hanauske, and S. Raha, Phys. Rev. C **71**, 048801 (2005).
[40] F. Yang and H. Shen, Phys. Rev. C **77**, 025801 (2008).
[41] A. Akmal, V. Pandharipande, and D. Ravenhall, Phys. Rev. C **58**, 1804 (1998).
[42] A. Douchin and P. Haensel, Astron. Astrophys. **380**, 151 (2001).
[43] S. K. Dhiman, R. Kumar, and B. K. Agrawal, Phys. Rev. C **76**, 045801 (2007).
[44] K. Sumiyoshi, H. Kuwabara, and H. Toki, Nucl. Phys. **A581**, 725 (1995).
[45] G. A. Lalazissis, J. Konig, and P. Ring, Phys. Rev. C **55**, 540 (1997).
[46] P. Rehberg, S. P. Klevansky, and J. Hüfner, Phys. Rev. C **53**, 410 (1996).
[47] N. Stergioulas and J. L. Friedman, Astrophys. J. **444**, 306 (1995).
[48] S. E. Thorsett and D. Chakrabarty, Astrophys. J. **512**, 288 (1999).
[49] J. W. T. Hessels, S. M. Ransom, I. H. Stairs, P. C. C. Freire, V. M. Kaspi, and F. Camilo, Science **311**, 1901 (2006).
[50] B. K. Agrawal and S. K. Dhiman, Phys. Rev. D **79**, 103006 (2009).